NPL

NPL REPORT MAT 60

Finite element analysis of the effect of residual stress on the distribution of stress and strain associated with a single pit

A Turnbull and L Crocker

August 2013

Finite element analysis of the effect of residual stress on the distribution of stress and strain associated with a single pit

Alan Turnbull and Louise Crocker
Materials Division

ABSTRACT

Previously, finite element analysis had been carried out to determine the stress and strain distribution associated with a single corrosion pit of varying geometry in a cylindrical specimen of steel stressed remotely in tension. In service, residual stresses are often present at the surface as a consequence of the surface finishing process and are known to impact on the likelihood of cracking. Relaxation of residual stress can occur when new free surface is created. The question then posed is the extent to which the residual stress and strain are redistributed in the presence of a pit. Assuming an axial tensile residual stress gradient near-surface induced by grinding, it is shown that the corrosion pit concentrates the stress in such a way that it becomes compressive local to the pit in the longitudinal direction while the tensile component increases in magnitude local to the pit in the transverse direction. When applied and residual stresses are combined to the extent that plasticity develops near the pit mouth, the maximum in tensile stress is shifted away from the pit mouth to the pit base. However, despite a high applied stress a compressive component still exists local to the pit mouth in in the longitudinal direction.

ISSN 1754-2979

National Physical Laboratory
Hampton Road, Teddington, Middlesex, TW11 0LW

Approved on behalf of the Managing Director, NPL,
by Dr Mark Gee, Knowledge Leader, Materials Division

CONTENTS

1 INTRODUCTION

Corrosion pits are often the precursor to stress corrosion cracks in power engineering, aerospace and oil and gas industries. This has prompted extensive modelling of pit and crack evolution [1-6] and more recently, effort to characterise the localisation of stress and strain associated with a pit using finite element (FE) analysis [7-9]. The latter enabled rationalisation of the experimental observation that cracks originated predominantly from near the pit mouth in low alloy and 12Cr martensitic stainless turbine steels in simulated steam condensate solution, though that observation should not be generalised. There has been increasing focus in stress corrosion cracking investigations on the impact of surface finish on the propensity for stress corrosion cracking. Surface grinding was shown to create a nanocrystalline surface layer, significant localised deformation, and potentially high levels of tensile residual stress [10]. Also, grinding often led to physical defects on the surface and these could be preferential sites for pit initiation. In the stress corrosion testing of the turbine steels, the steels were stress relieved; hence, residual stress was not an issue in that case. However, in many applications, residual stress can potentially have an impact, yet the interrelationship between residual stress and a corrosion pit in terms of the local stress and strain distribution is unclear. In particular, what is the balance between stress localisation due to the pit acting as a stress concentrator and stress relaxation because of the generation of free surface. To model a real system comprehensively using finite element analysis is a major challenge because account has to be taken of the change in local mechanical properties near surface associated with the heavy deformation and nanocrystalline layer. Since the purpose of this exercise is to gain physical insight rather than to make explicit quantitative predictions for a particular ground surface we simplify the problem by considering the material containing the single pit to be homogeneous in both bulk and near surface material properties but with a gradient in residual stress imposed. In addition to considering residual stress in isolation the effect of a combination of residual and applied stress was examined.

2 MATERIAL PROPERTIES AND STRESS CONDITIONS

To align with previous work [9] we assume a turbine blade steel, FV566, with mechanical properties as given in Table 1. The test temperature reflects the temperature of the early condensate on a low pressure steam turbine.

Table 1 Mechanical properties (mean values) of the FV566 steel

Condition	T (°C)	E (GPa)	$\sigma_{0.2}$ (MPa)	UTS (MPa)	Elongation (%)
Stress relieved	90	210	819	911	20.5

Poisson's ratio for the steel was not measured and a value of 0.3 was adopted.

The analysis makes use of the full stress-strain behaviour of the material and a plot of the data is shown in Figure 1.

3 BASIS OF FINITE ELEMENT ANALYSIS

The FE analysis has been carried out using ABAQUS V6.11-3. A 3-D version of the cylindrical specimen was modelled in the ABAQUS CAE pre-processor (see Reference 8 for more details). A pit was created halfway along the length of the specimen.

The mesh was created using the 3-D elements C3D4, which are 4-node linear tetrahedral elements. The mesh was refined in the region around the pit to enhance the accuracy of stress and strain predictions (Figure 2).

Boundary conditions were applied to the ends of the specimen to ensure specimen alignment during loading. A uniform stress was applied to the surface at one end of the specimen. The von Mises material model was used in the analysis to characterise the elastic-plastic behaviour of the material.

4 SPECIMEN GEOMETRY

The specimen diameter was 6.4 mm. Calculations were performed for a 100 μm deep pit. For the truncated sphere of the pit this corresponded to a pit radius of 65 μm and mouth opening of 110 μm.

5 RESIDUAL AND APPLIED STRESS

The residual stress was assumed to have a maximum axial tensile component at the surface of 626.2 MPa, corresponding to about 76% of $\sigma_{0.2}$ (in the elastic region of the stress-strain curve), and to vary linearly with depth from the outer radius r=R (Figure 3) to the inner radius r=a. The distance R-a was taken to be 200 μm. Within the inner radius, the stress was compressive and constant with a value of -21.36 MPa. The compressive stresses have to balance the tensile stresses in the system. Defining the tensile stress gradient as above then the compressive stress (σ_c) must then be given by:

$$\sigma_c = \left[\frac{R^2 - a^2}{a^2}\right] \sigma_t^{mean}$$

where σ_t^{mean} is the mean value of the tensile stress. Here, it is assumed that the compressive stress is uniform in the region bounded by the tensile residual stress.

A user subroutine was written enabling this definition of the initial stress distribution to be applied to the cylinder.

In appropriate cases a remote applied stress corresponding to either 30% or 90% of $\sigma_{0.2}$ was superimposed on the residual stress.

6 RESULTS AND DISCUSSION

6.1 RESIDUAL STRESS ONLY

Representations of the local stress and strain distribution around the pit in response to the residual stress only are shown in Figures 4-7. To gauge the extent of local plasticity, it should be noted that the strain at the proportional limit is about 3.4×10^{-3}. Figure 4 shows that the tensile residual stress is elevated in the transverse direction immediately adjacent to the pit while in the longitudinal direction the residual stress becomes compressive. This is not surprising as there has to be a stress balance in the system. Relaxation of tensile residual stress also occurs to an extent at a distance from the pit[1]. In the absence of local stress concentrators, residual stresses are inherently elastic. However, in the presence of a pit, which acts as a stress raiser, the strain local to the pit can exceed the proportional limit and plasticity ensues, seen most clearly in Figure 7. In previous analysis [7], in which only applied stress was accounted for, the effect of plasticity at the pit mouth was to shift the maximum stress away from the mouth. However, this was not apparent in this study for which residual stress only was present; the stress gradient perhaps providing the dominant influence.

It should be recalled that this is a model system with residual stress introduced notionally through surface grinding but without the near-surface change in microstructure that might be associated with that process. Any near-surface variation in mechanical properties as a consequence of that change in

1 The reduced mesh density away from the pit can result in more uncertainty (noise) in the calculated stress and this accounts for the unusual feature in the top right hand corner of this figure.

microstructure would impinge on the onset of plasticity and the redistribution of stress. Hence, the analysis undertaken here should be considered indicative at this stage. Advanced modelling embracing the near-surface gradient in mechanical properties is required to enable more realistic prediction of the stress and strain distribution. Nevertheless, the trend would be the same. The effect of a higher yield strength near surface would simply defer the onset of yielding until the pit size was larger.

6.2 RESIDUAL + APPLIED STRESS

At an applied stress of 30% of $\sigma_{0.2}$ the most distinctive feature (Figure 8) of the stress distribution is that the stress is neither a maximum at the mouth nor at the base but in between. Notably, there is still significant compressive stress in the longitudinal direction, Figure 9. The shift in position of maximum tensile stress local to the pit to further from the pit mouth would seem to reflect the increased extent of plasticity near the mouth of the pit (compare the magnitude of the strain near the pit mouth in Figure 10 and Figure 7) and redistribution of the stress.

Increasing the applied stress to 90% of $\sigma_{0.2}$ causes the maximum stress to move further towards the pit base (Figure 11) although the maximum is only slightly above that for an applied stress of 30%. The main difference appears to be a greater spread in plasticity, with the maximum strain again near the pit mouth (Figure 12). Interestingly, despite the high applied stress, there is still a small compressive stress local to the pit along the length of the specimen, as shown in Figure 13.

7 CONCLUSIONS

Pitting in a material with a near-surface gradient in tensile residual stress will cause the local tensile stress round the pit to be elevated in the transverse direction immediately adjacent to the pit and the stress in the longitudinal direction to become compressive.

The stress tended to be a maximum at the pit mouth, reflecting primarily the pre-existing stress gradient.

In the presence of a superimposed applied stress, increased plasticity caused the stress maximum to move away from the pit mouth and to move increasingly towards the pit base with increasing magnitude of the applied stress.

Compressive stresses persisted local to the pit in the longitudinal direction despite an applied stress of 90% $\sigma_{0.2}$.

8 REFERENCES

(1) Kondo, Y., Corrosion, 45 (1989) 7.
(2) Wei, RP, Material aging and reliability of engineered systems, Proceedings of conference on Environmentally Assisted Cracking: Predictive methods for risk assessment and evaluation of material, equipment and structures, Ed. R.D. Kane, ASTM STP1401, 2000, pp. 3-19.
(3) Engelhardt, G, Macdonald, DD, Zhang, Y and Dooley, B, Power Plant Chemistry, 6 (2004) 647.
(4) Engelhardt, G and Macdonald, DD, Unification of the deterministic and statistical approaches to prediction localised corrosion damage – The theoretical foundations, Corros. Sci., 46 (2004) 2755.
(5) Turnbull, A, McCartney, LN and Zhou, S, Corros. Sci., 48 (2006) 2084.
(6) Turnbull, A, McCartney, LN and Zhou, S, Scripta Materialia, 54 (2006) 575.
(7) Turnbull, A and Crocker, L, Finite element analysis of the stress and strain associated with a corrosion pit in a cylindrical specimen under applied tensile loading, NPL Report DEPC-MPE 034, 2006.
(8) Turnbull, A, Wright, L and Crocker, L, Corros. Sci., 52 (2010) 1492.
(9) Turnbull, A and Crocker, L, Finite element analysis of the effect of pit shape on the local stress and strain distribution, NPL Report MAT 51, 2011.
(10) Turnbull, A, Mingard, K, Lord, JD, Roebuck, B, Tice, D, Mottershead, K, Fairweather, N, Bradbury, A, Corros. Sci. 53 (2011) 3398.

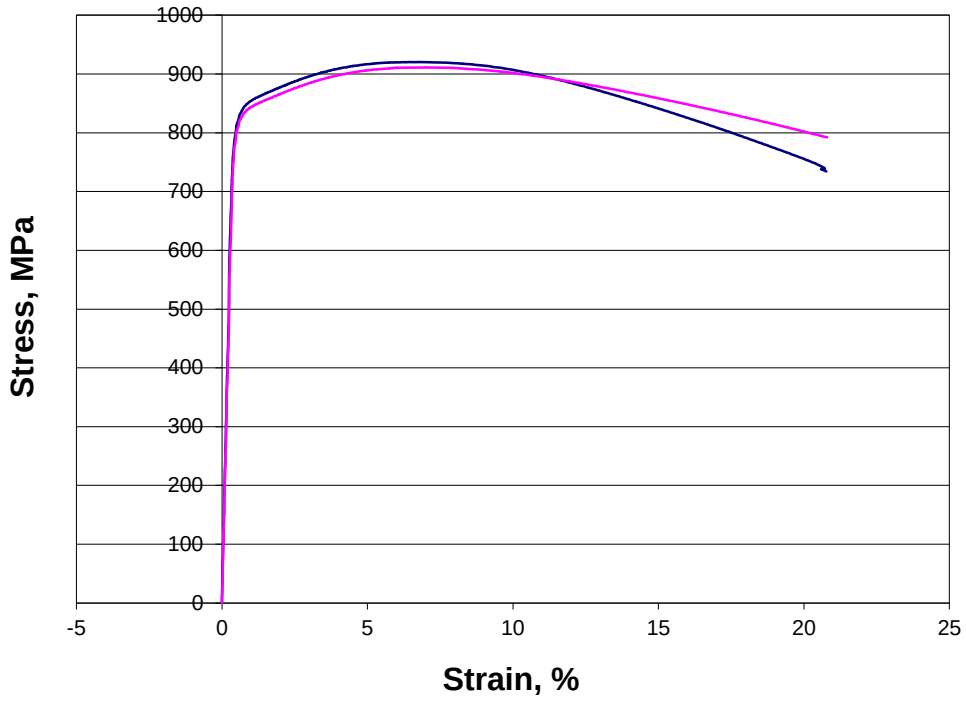

Figure 1: Stress-strain behaviour for a FV566 steel in air at 90 °C.

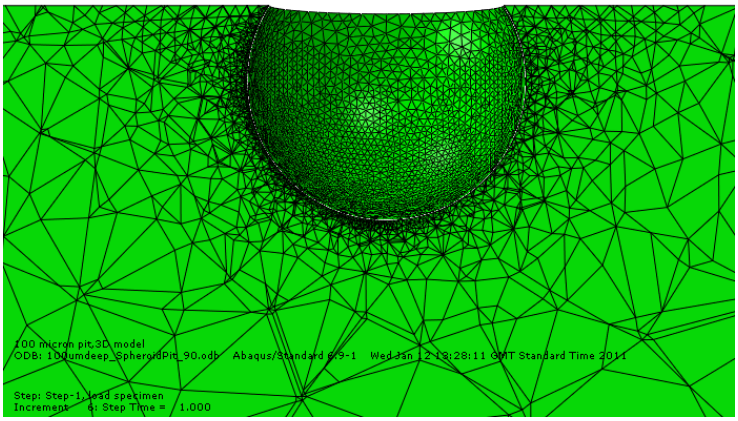

Figure 2: Pit geometry showing meshing for 100 μm deep truncated-spherical pit.

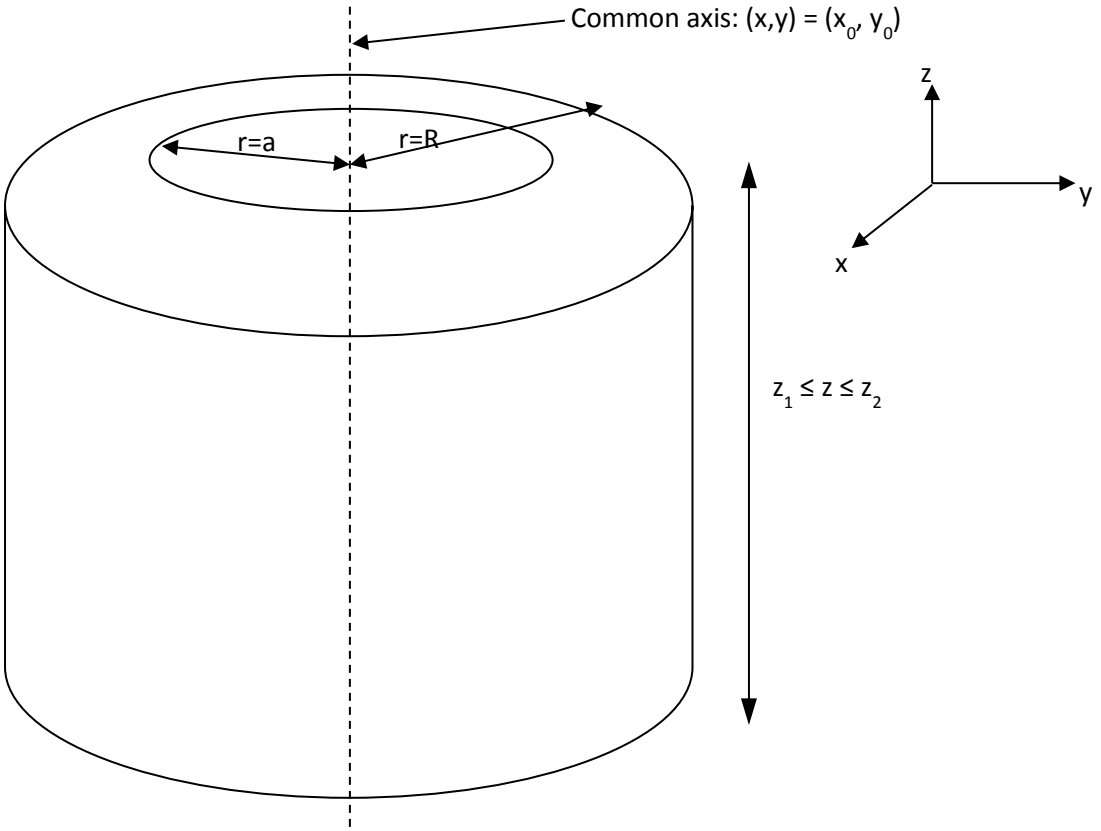

Figure 3: Residual stress was assumed tensile in region r=R-a and compressive in region r=a.

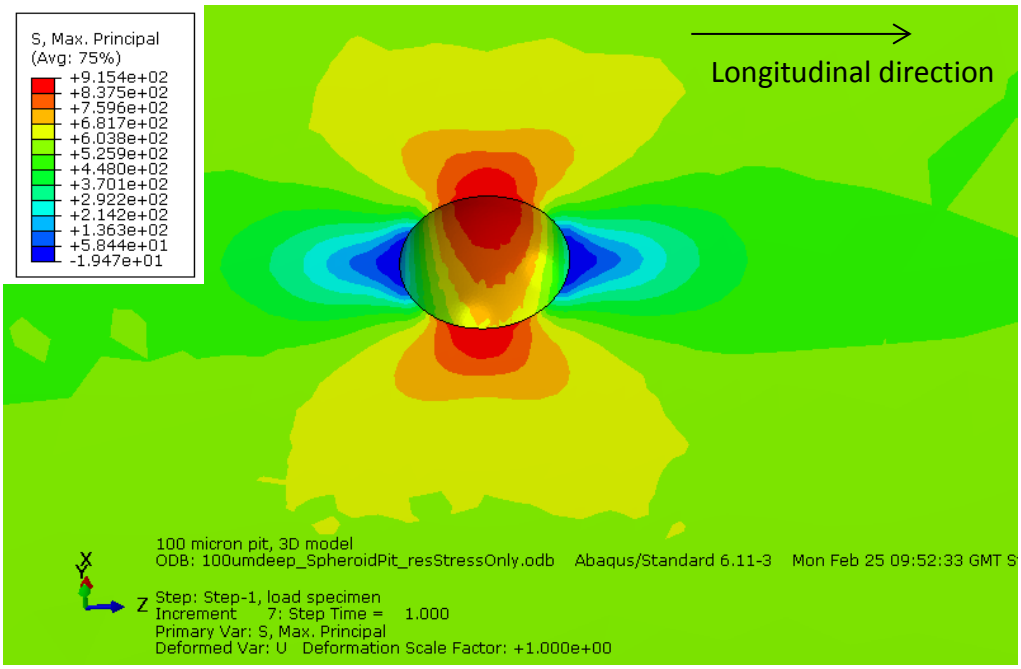

Figure 4: Maximum principal stress in 3D view.

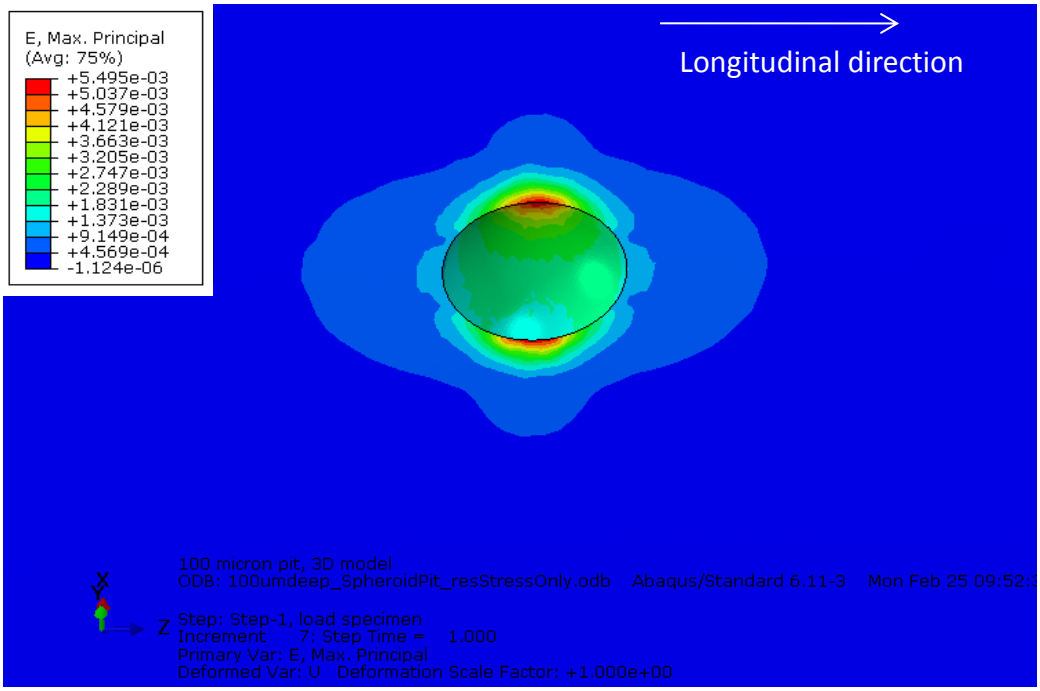

Figure 5: Maximum principal strain in 3D view.

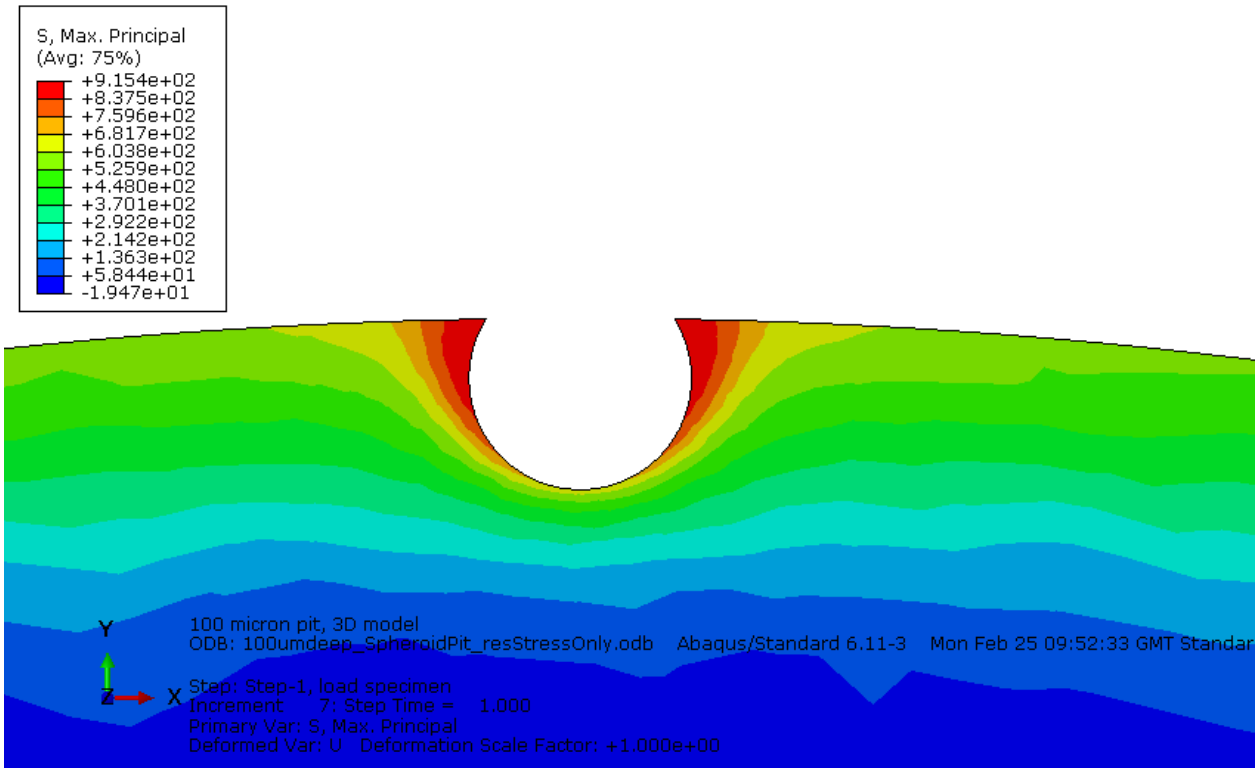

Figure 6: Maximum principal stress, cross-section view.

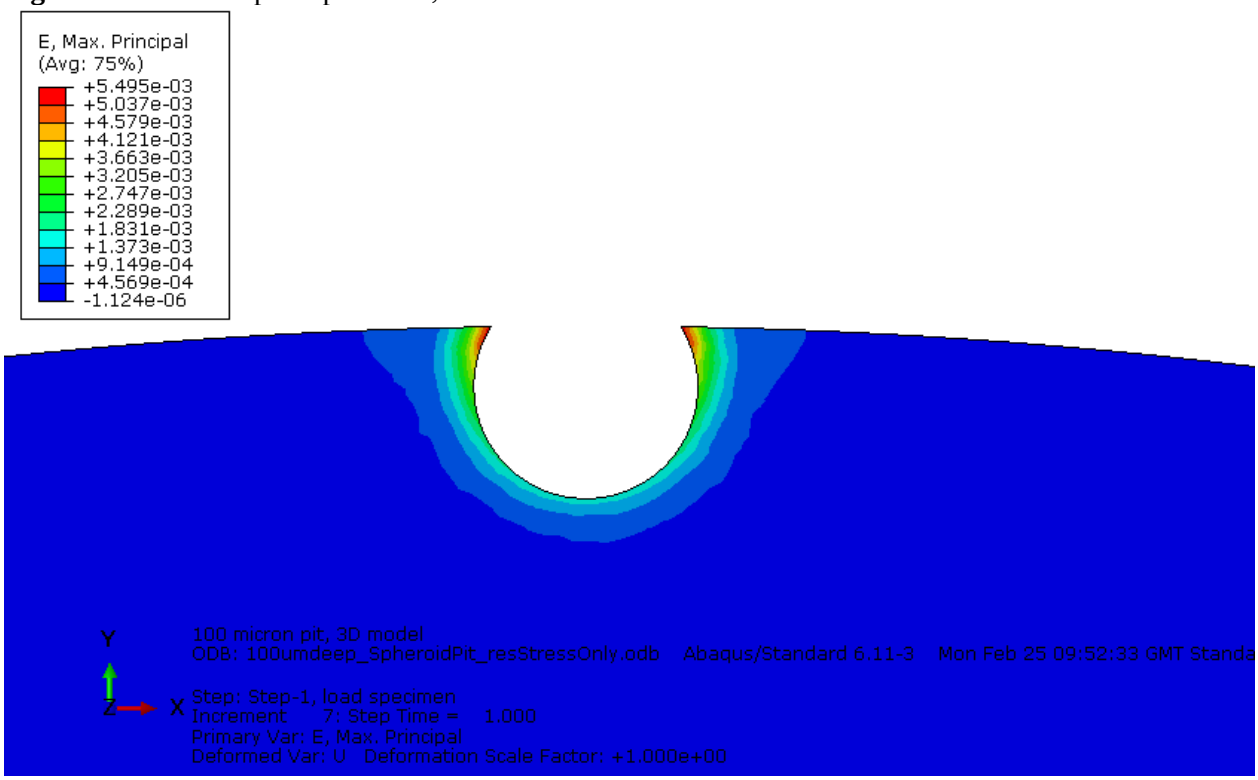

Figure 7: Maximum principal strain, cross-section view.

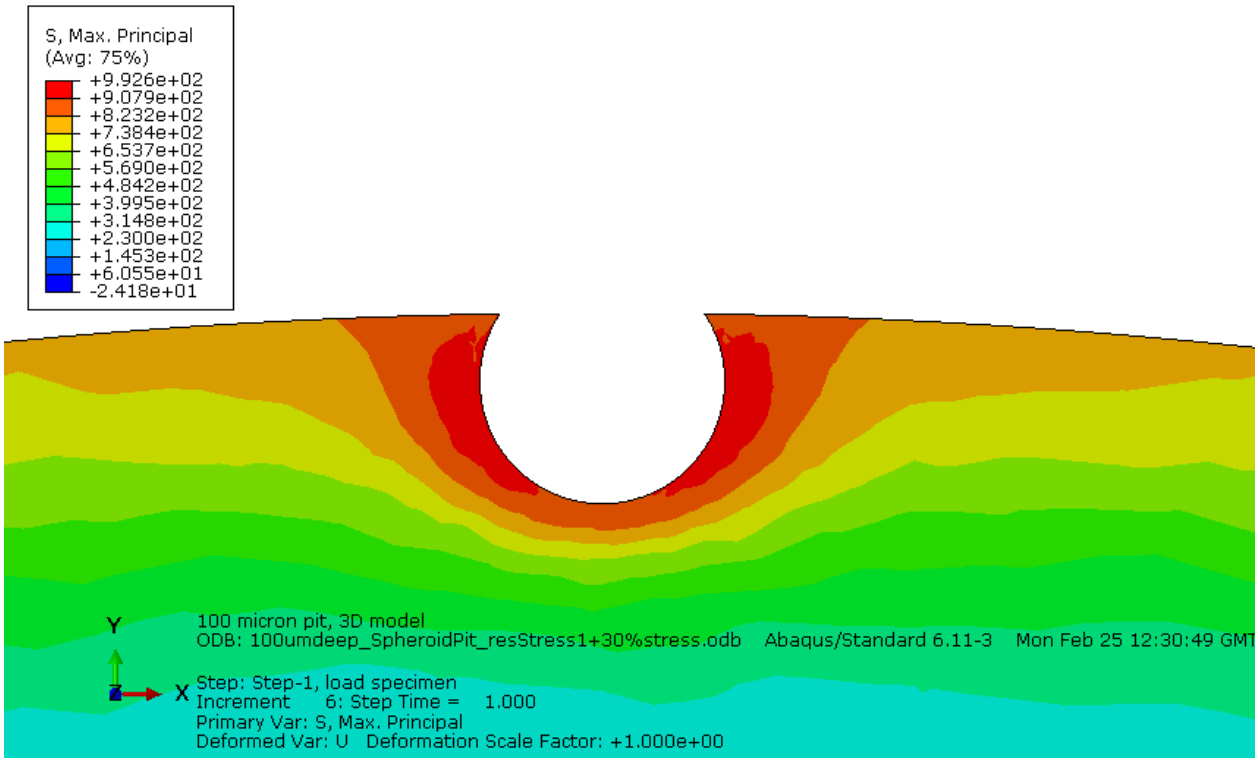

Figure 8: Maximum principal stress, cross section view, with applied stress of 30% $\sigma_{0.2}$ superimposed on residual stress.

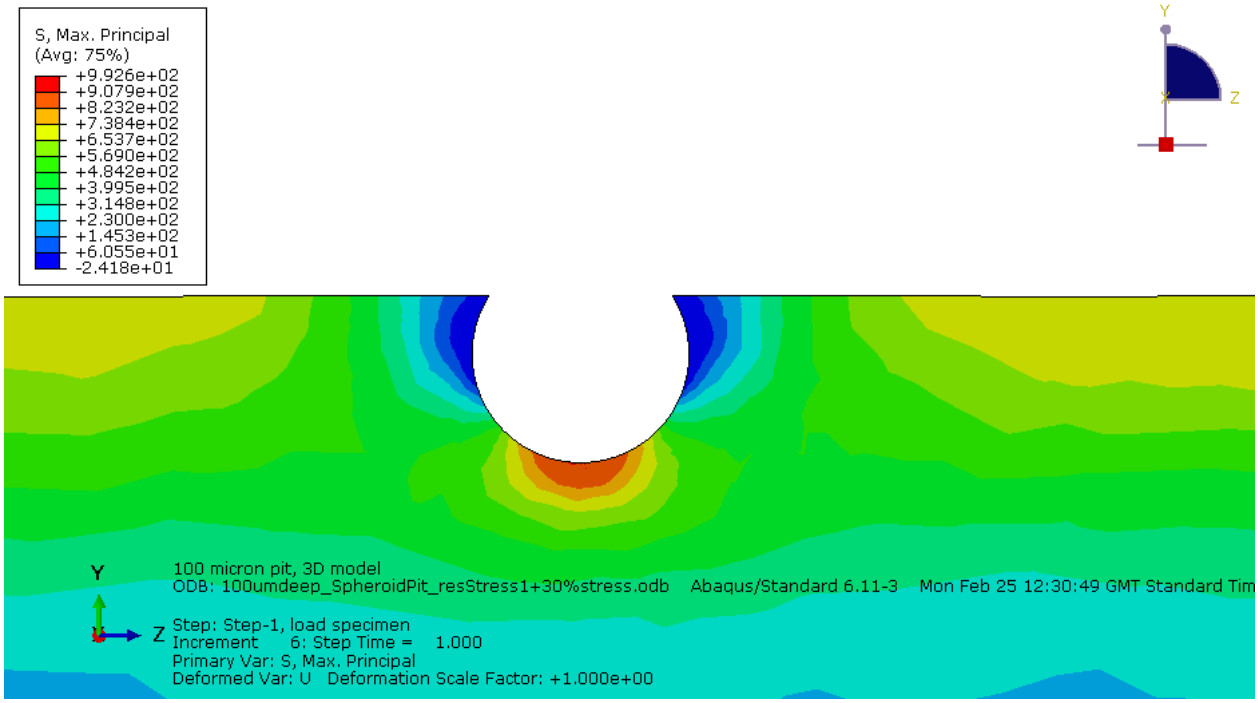

Figure 9: Maximum principal stress, longitudinal section, with applied stress of 30% $\sigma_{0.2}$ superimposed on residual stress.

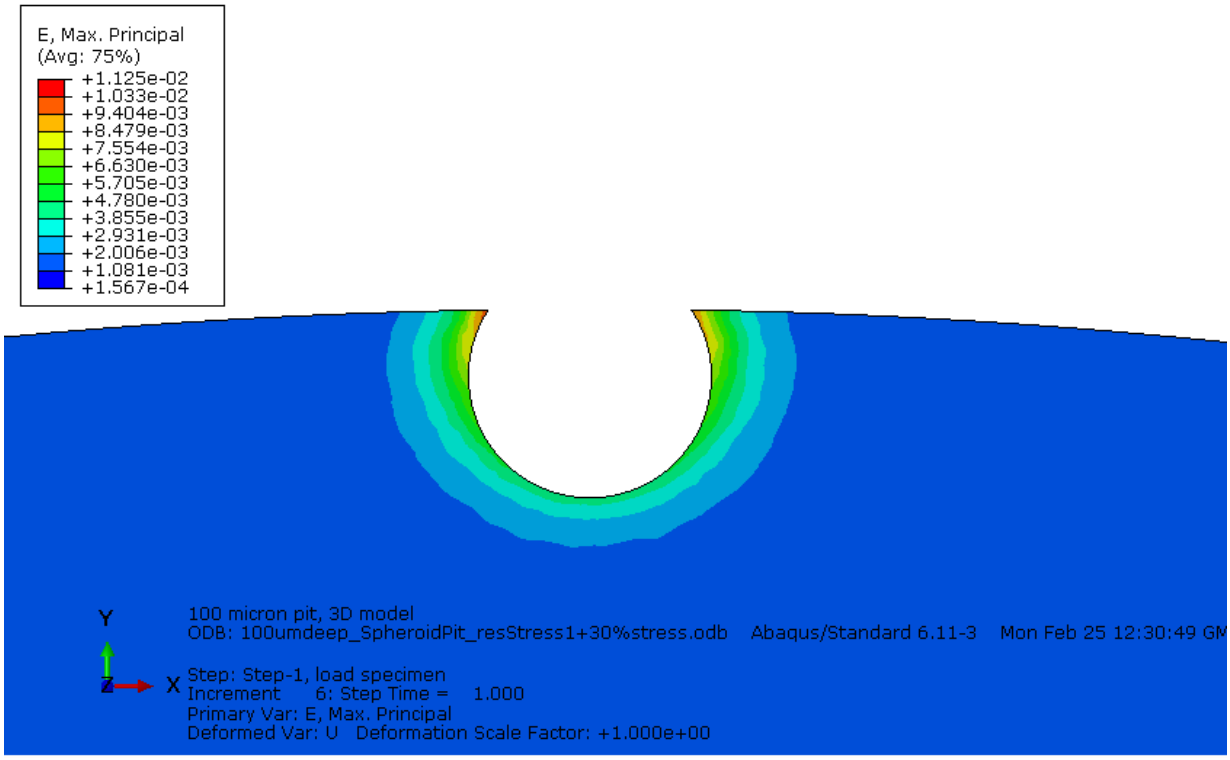

Figure 10: Maximum principal strain, cross section view, with applied stress of 30% $\sigma_{0.2}$ superimposed on residual stress.

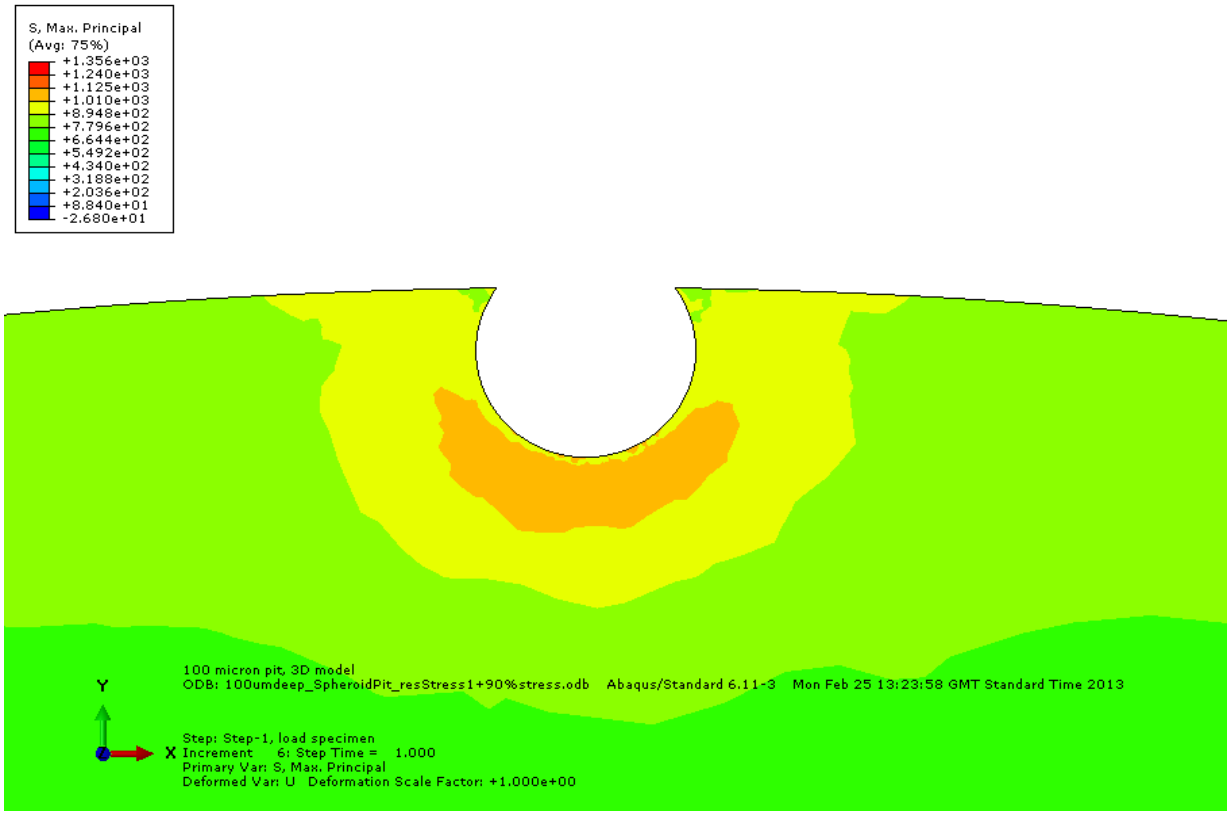

Figure 11: Maximum principal stress, cross section view, with applied stress of 90% $\sigma_{0.2}$ superimposed on residual stress.

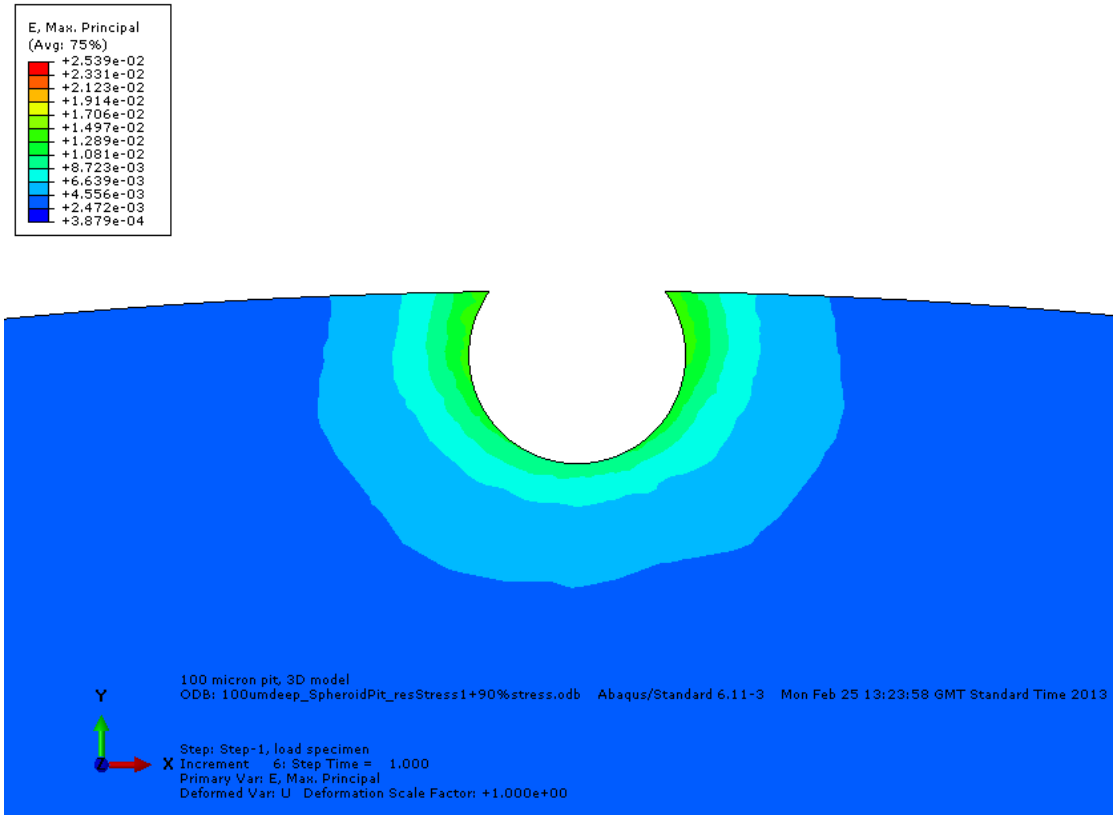

Figure 12: Maximum principal strain, cross section view withapplied stress of 90% $\sigma_{0.2}$ superimposed on residual stress.

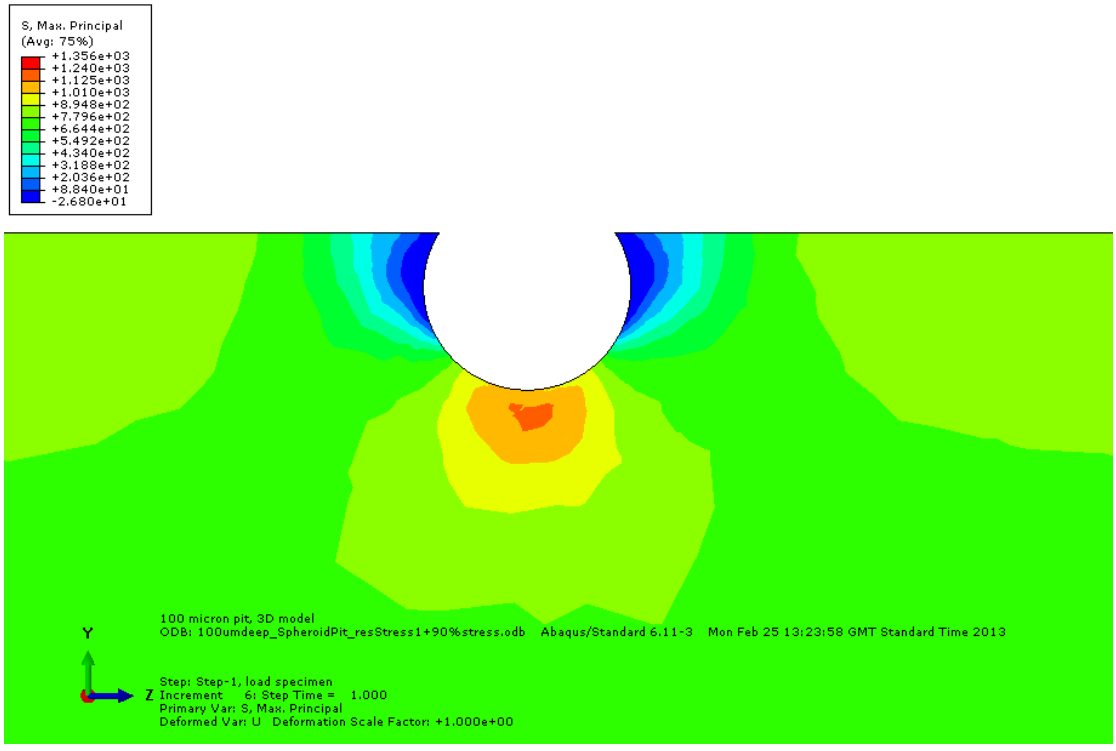

Figure 13: Maximum principal stress, longitudinal view, with applied stress of 90% $\sigma_{0.2}$ superimposed on residual stress.